Vortex head-to-head domain walls and their formation in onion-state ring elements

M. H. Park,[1] Y. K. Hong,[1] B. C. Choi,[2] M. J. Donahue,[3] H. Han,[1] and S. H. Gee[1]
[1]*Department of Materials Science and Engineering, University of Idaho, Moscow, Idaho 83844, USA*
[2]*Department of Physics and Astronomy, University of Victoria, Victoria, BC, Canada V8W 3P6*
[3]*Mathematical & Computational Sciences Division, National Institute of Standards and Technology, Gaithersburg, Maryland 20899, USA*
(Received 14 December 2005; published 20 March 2006)

Magnetization configuration of vortex head-to-head (HTH) domain walls and the wall-formation process in $Ni_{80}Fe_{20}$ ring elements were investigated using magnetic force microscopy (MFM) and micromagnetic simulation. At remanence, two types of vortex HTH domain walls were observed to be stable in the onion configuration, depending on the film thickness: single- and double-vortex HTH domain walls for 40 and 65 nm thick ring elements, respectively. As the vortex core nucleated during formation of the HTH domain wall, exchange energy began to decrease, accompanied by an increase in the width of the wall. Vortex nucleation in the 65 nm thick ring was found to be much faster than in the 40 nm thick ring element. This effect can be attributed to the higher initial magnetostatic energy density in the thicker ring.

DOI: 10.1103/PhysRevB.73.094424 PACS number(s): 75.60.Ch, 75.60.Ej

Small ferromagnetic ring elements have received considerable attention in recent years due to their possible applications in memory devices and magnetic sensors.[1–3] In ring elements, two stable domain configurations, i.e., vortex and onion states, have been observed with an in-plane applied field.[3–5] The onion state, which is defined as a ring domain configuration with two head-to-head (HTH) (or, more precisely, one HTH and one tail-to-tail) domain walls, is being explored for application as a bit state of magnetic memory devices because it is easy to control the domain configuration with in-plane magnetic fields. Magnetization configurations in ring elements are found to depend strongly on ring geometry, so desirable characteristics can be fabricated by design.[5,6]

For the onion-state ring element, it is believed that the HTH domain-wall configuration plays an important role in the switching behavior of the ring element because switching is driven by annihilation and nucleation of HTH domain walls.[6–10] Two types of HTH domain walls in thin film ring elements and narrow strips are well known: transverse and vortex walls.[10–13] Transverse domain walls are generally observed in thin and narrow wires, and the spin configuration of the wall appears as a "V" shape with two 90° (Néel) walls. On the other hand, the vortex-type domain wall shows a twofold rotational symmetry about its vortex center, resembling an N-shaped magnetic spin configuration. This type of HTH domain wall is typically observed in relatively thick and wide wires. In addition to these known HTH domain walls, other possible HTH domain-wall configurations may exist, such as the multivortex plus cross-tie domain wall in a ring element or narrow strip as suggested by McMichael and Donahue.[11] However, it seems that these types of HTH domain walls have not been experimentally investigated. Buntinx *et al.* (refer to Fig. 2(a) in Ref. 14) provide a MFM image of a 35 nm thick $Ni_{80}Fe_{20}$ ring with an outer diameter of 5 μm and a width of 0.5 μm that shows a double-vortex HTH wall, but that structure was not identified.

In this work, we use MFM and micromagnetic simulation to study single- and double-vortex HTH domain walls in $Ni_{80}Fe_{20}$ rings with various inner hole diameters and two film thicknesses. We also discuss the contribution of exchange and demagnetizing energies on the formation of HTH domain walls.

In our experiments, 2 μm o.d. ring-shaped $Ni_{80}Fe_{20}$ elements with various ratios of inner-to-outer diameters ($D_{I/O}$) and thicknesses were patterned. Ferromagnetic films composed of Ta (5 nm)/NiFe(t nm)/Ta(5 nm) with thickness t of 40 or 65 nm were sputtered on Si substrates. Ring elements were patterned using electron-beam lithography with a negative resist and ion milling. Figure 1 shows scanning electron microscope images of fabricated elements. The ring dimensions of each column are shown in Table I. Magnetization configurations of the ring elements were observed by MFM, operated in tapping-lift mode, and oscillating at its resonant frequency. The MFM tips used were commercially available low-moment tips with a $Co_{80}Cr_{20}$ coating of ~15 nm thickness in order to minimize the tip-induced perturbations on the patterned elements. The tip was magnetized in the z direction; the lift height was over 50 nm.

Figure 2 shows the MFM images of the ring elements at remanent state, after saturating to 400 kA/m (5 kOe) along the $+y$ direction. As seen in the figures, the onion state becomes unstable as $D_{I/O}$ decreases or film thickness increases. This is because the demagnetizing energy increases with decreasing $D_{I/O}$ or increasing film thickness until the onion

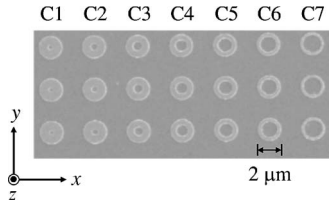

FIG. 1. SEM images of $Ni_{80}Fe_{20}$ ring elements with D_O = 2.0 μm. The thickness of each ring element shown is 40 nm. The rings in the same column have the same dimensions (see Table I).

TABLE I. Dimensions of the ring elements shown in Fig. 1.

Columns		C_1 (μm)	C_2 (μm)	C_3 (μm)	C_4 (μm)	C_5 (μm)	C_6 (μm)	C_7 (μm)
D_O=2.0 μm	D_I	0.4	0.6	0.8	1.0	1.2	1.4	1.6
	$D_{I/O}$	0.2	0.3	0.4	0.5	0.6	0.7	0.8

state is no longer stable and only the vortex ring configuration (circular pattern with no domain walls) is accessible. The dependence of the energies for equilibrium states on $D_{I/O}$ and thickness t is summarized in Table II for selected elements. Each study was performed by initially making an arrangement of spins into a configuration containing a single- or double-vortex wall, and then followed by conjugate-gradient minimization until a local energy minimum was reached. As seen in Table II, the exchange energy also increases with decreasing inner radius or increasing film thickness. In order to compensate the wall twists even tighter, the demagnetization increases and, consequently, the exchange energy increases. The single-vortex wall at t =65 nm, $D_{I/O}$=0.6 was not stable in the simulation. In experiments, a stable onion ring configuration is observed in the 40 nm thick ring elements with $D_{I/O}>0.4$ and in the 65 nm thick ring elements with $D_{I/O}>0.5$. A similar geometric dependence in the ring magnetization configuration has been reported previously.[5,6]

Note that in Fig. 2, the HTH domain-wall structure of onion-state ring elements changes with thickness. There exist two magnetic poles in each HTH domain wall in the 40 nm thick ring elements, while for the 65 nm cases three magnetic poles are observed in each HTH domain wall. In order to investigate the detailed magnetization configuration of the onion-state ring elements, the results of micromagnetic simulations[15]for 40 and 65 nm thick ring elements with $D_{I/O}$=0.6 are presented in Figs. 3(a) and 3(b), respectively. Figures 3(c) and 3(d) show the corresponding MFM images, which were rescanned at a higher resolution.

In both cases, i.e., modeling and MFM imaging, the magnetization configurations shown are remanent states arising after applying a 400 kA/m (5 kOe) field directed along the $-y$ axis. The parameters used in the simulations were: saturation magnetization M_S=800 kA/m, exchange stiffness A =10 pJ/m, zero magnetocrystalline anisotropy, and damping constant α=0.1. The unit cell volume was 5 nm$\times$5 nm$\times t$, where t is the film thickness. One arrow represents a group of 24$\times$24 basic cells (i.e., 120 nm$\times$120 nm) for a better

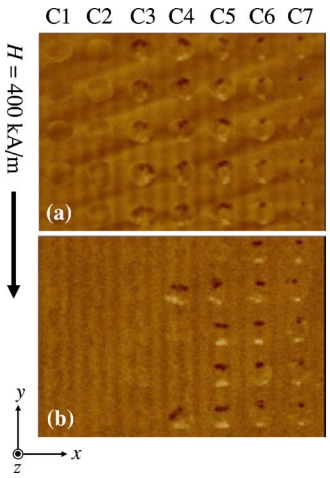

FIG. 2. (Color online) MFM images of ring elements with a thickness of (a) 40 nm and (b) 65 nm at remanent states after saturating at 5 kOe. $C_1 \sim C_7$ represent the column numbers corresponding to Fig. 1.

visual presentation. Outside of the vortex cores, the magnetization lies essentially in plane. The color of the magnetic cells in Figs. 3–5 represents the divergence of the magnetization. Deepening red indicates increasingly positive divergence (corresponding to negative magnetic charge), whereas blue indicates negative divergence (positive charge). Although the absolute color contrast on the simulated images may be different from the real pole strength, the qualitative results are well matched with experimental results. The simulation results imply that the 40 nm thick ring elements showing two magnetic poles on each HTH domain wall possess single-vortex HTH domain walls, while the 65 nm thick ring elements showing three magnetic poles have double-vortex HTH domain walls. The z-axis (i.e., out of the page) component of magnetic flux from the vortex cores inside the HTH domain walls, however, could not be resolved in our MFM measurements. We note that the asymmetry between extensions of the magnetic domains in the two ring branches in Fig. 3(d) is due to the presence of geometric asymmetries in the ring elements.[7] The distribution of the angle between the two double-vortex HTH wall positions due to the minor geometric asymmetries is evident in Fig. 2. In these cases the two walls are only weakly interacting, and thus it does not take much a slight misalignment of the hole to move one wall relative to the other. In our simulation for Fig. 3(b), which is found to agree well with the experiment, we assumed a gradual variation of the ring width in which the

TABLE II. Dependence of the energies for equilibrium states on $D_{I/O}$ and thickness t.

		One-vortex wall			Two-vortex wall		
Thickness t (nm)	$D_{I/O}$	$E_{Exchange}$ (10^{-16} J)	E_{Demag} (10^{-16} J)	E_{Total} (10^{-16} J)	$E_{Exchange}$ (10^{-16} J)	E_{Demag} (10^{-16} J)	E_{Total} (10^{-16} J)
40	0.6	0.7410	3.8575	4.5985	1.0506	3.3694	4.4201
	0.8	0.5076	2.2939	2.8016	0.74784	2.0910	2.8389
65	0.6				2.0479	7.1875	9.2354
	0.8	1.1477	4.5420	5.6898	1.3528	4.1885	5.5414

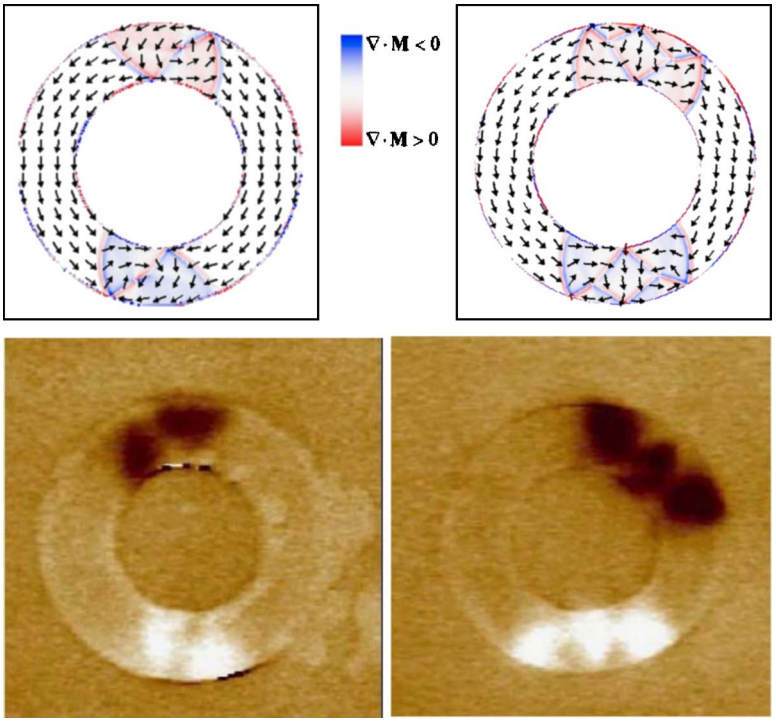

FIG. 3. (Color online) Micromagnetic simulations showing magnetic spin configurations of 2 μm size $Ni_{80}Fe_{20}$ ring elements obtained at remanent states after saturation (H_{app}=5 kOe) along with y axis for (a) $D_{l/O}$=0.6, t=40 nm and for (b) $D_{l/O}$=0.6, t=65 nm. (c) and (d) are the corresponding MFM images rescanned with a higher resolution for t=40 nm and t=65 nm, respectively. The blue color indicates the divergence of magnetization along $+z$ direction while red means the ones along $-z$ direction.

right-hand side of the element is ~3% narrower than the left-hand side. Since the simulation lacks defects other than the negligible edge roughness, the stronger asymmetry in the element shape leads the domain walls to collapse into the no-wall state.

The formation process of the vortex HTH domain wall in ring elements with $D_{l/O}$=0.6 was also investigated by micromagnetic simulations. Snapshots showing the vortex nucleation process for 40 and 65 nm thick ring elements are presented in Figs. 4 and 5, respectively, and the corresponding energy variations as a function of time are shown in Figs. 6(a) and 6(b). The initial states are formed by relaxing the magnetization to equilibrium in a 400 kA/m (5 kOe) field applied along the $-y$ direction. At time zero the applied field is removed and then the magnetization configuration is relaxed to remanence. In both cases, Figs. 4 and 5, Néel-like 180° HTH domain walls are initially formed. These walls quickly split into two V-shaped 90° Néel walls, similar to the transverse HTH domain wall. Then, vortices nucleate on the outer edge of the ring, dramatically reducing the demagnetizing energy. For a 65 nm thick ring element, two vortices form, simultaneously, and move to the outer corners of the V-shaped 90° Néel walls. The reduction of demagnetizing energy is found to be greater than in the case of the 40 nm

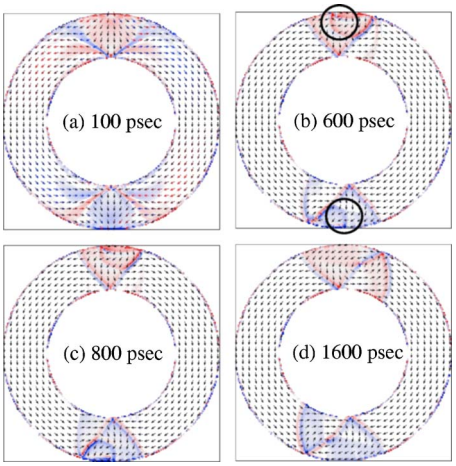

FIG. 4. (Color online) Snapshots showing vortex HTH domain-wall nucleation of 40 nm thick ring elements with $D_{l/O}$=0.6. A saturating magnetic field was applied along an in-plane direction and relaxed to zero field. The blue color indicates the divergence of magnetization along $+z$ direction while red means the ones along the $-z$ direction.

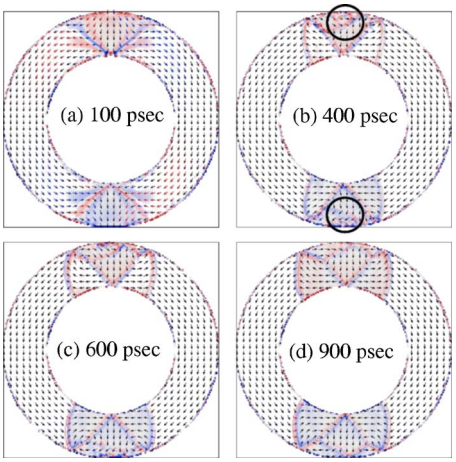

FIG. 5. (Color online) Snapshots showing vortex HTH domain-wall nucleation of 65 nm thick ring elements with $D_{l/O}$=0.6. A saturating magnetic field was applied along an in-plane direction, and relaxed to zero field. Blue indicates the divergence of magnetization along $+z$ direction while red means the ones along $-z$ direction.

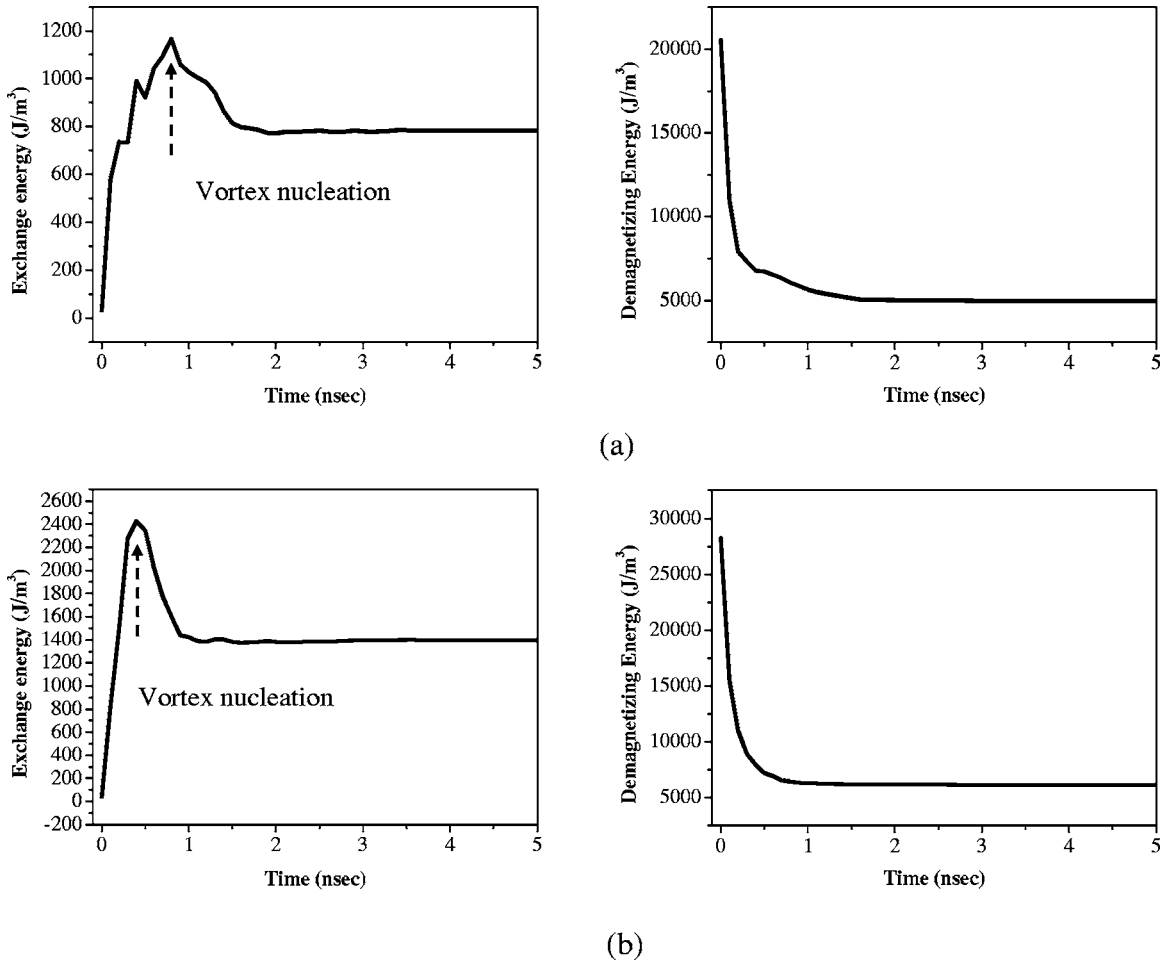

FIG. 6. Average exchange and demagnetizing energy densities during nucleation of single- and double-vortex HTH domain walls in (a) 40 and (b) 65 nm thick ring elements with $D_{I/O}=0.6$.

thick ring element, where only a single vortex is nucleated. In both cases, once the vortices reach the Néel walls, they move along the walls toward the center of the HTH domain wall and complete the wall formation process. It should be noted that the domain walls grow wider in both cases once the vortex cores are nucleated. Vortex nucleation coincides with a peak in the exchange energy, as indicated by the arrows in Fig. 6.

As seen in the simulation results, the 65 nm thick ring element has a higher average demagnetizing energy density (28 244 J/m^3) than the 40 nm thick ring element (20 566 J/m^3) in the initial relaxed saturation state. Because of the higher domain-wall energy in the 65 nm thick ring element, the driving force in the domain-wall transformation should be much greater than in the 40 nm thick ring element, and the nucleation process should occur faster. Indeed, for 65 nm thick ring elements, vortices are nucleated at 400 ps and the formation of the double-vortex HTH domain wall is completed in 900 ps; whereas, for 40 nm thick ring elements, vortices are nucleated at 600 ps and the formation of the single-vortex HTH domain wall requires 1500 ps [refer to the exchange energy graph in Figs. 6(a) and 6(b)].

As shown in Figs. 4 and 5, it is observed that the vortex nucleation occurred along the outer edges of the ring elements during the HTH domain-wall formation process. The nucleation sites are indicated by circles in the figures. Those sites did not play an otherwise important role in the further formation of the vortex domain walls. However, in some simulations with thicker films, more complex vortex formation occurs, resulting in HTH domain walls with cross-ties and more than two vortices. Although we have not experimentally observed these types of domain walls, the simulations suggest that other types of HTH domain walls may exist in patterned ring elements.

In summary, the magnetization configuration and nucleation process of vortex HTH domain walls in onion-state ring elements were investigated by MFM and micromagnetic simulation. In both simulations and experiments, single-vortex HTH domain walls were found in 40 nm thick ring elements, whereas in 65 nm thick ring elements double-vortex HTH domain walls were preferred. During the transition from saturation to remanence, the initial Néel-like 180° HTH domain wall splits into a V-shaped transverse domain wall composed of two 90° Néel walls. At this point, vortex cores are nucleated near the outer corners of the V-shaped walls, and then move along the wall toward the center of the wall. During this process, the domain wall grows wider, resulting in a decrease in the exchange energy. Therefore, the peak point in the exchange energy vs time graph indicates

the nucleation of the vortex core. Simulations indicate that the vortex nucleation process was faster in 65 nm thick ring elements, and that this is due to a higher initial demagnetizing energy, as compared to the 40 nm thick ring elements. Some of the simulations produced HTH domain walls with multiple vortices separated by cross-ties, suggesting that other wall configurations are possible; however, these more complex walls were not experimentally observed.

This work was supported by Office of Naval Research under Contract No. N00014-02-1-0991.

[1] J. G. Zhu, Y. Zheng, and G. A. Prinz, J. Appl. Phys. **87**, 6668 (2000).
[2] M. M. Miller, G. A. Prinz, S.-F. Cheng, and S. Bounnak, Appl. Phys. Lett. **81**, 2211 (2002).
[3] M. Kläui, C. A. F. Vaz, L. Lopez-Diaz, and J. A. C. Bland, J. Phys.: Condens. Matter **15**, R985 (2003).
[4] S. Kasai, T. Niiyama, E. Saitoh, and H. Miyajima, J. Magn. Magn. Mater. **239**, 228 (2002).
[5] M. Steiner and J. Nitta, Appl. Phys. Lett. **84**, 939 (2004).
[6] F. J. Castaño, C. A. Ross, A. Eilez, W. Jung, and C. Frandsen, Phys. Rev. B **69**, 144421 (2004).
[7] J. Rothman, M. Klaui, L. Lopez-Diaz, C. A. F. Vaz, A. Bleloch, J. A. C. Bland, Z. Cui, and R. Speaks, Phys. Rev. Lett. **86**, 1098 (2001).
[8] M. Kläui, C. A. F. Vaz, J. A. C. Bland, W. Wernsdorfer, G. Faini, and E. Cambril, Appl. Phys. Lett. **81**, 108 (2002).
[9] M. Kläui, C. A. F. Vaz, J. A. C. Bland, T. L. Monchesky, J. Unguris, E. Bauer, S. Cherifi, S. Heun, A. Locatelli, L. J. Heyderman, and Z. Cui, Phys. Rev. B **68**, 134426 (2003).
[10] M. Kläui, C. A. F. Vaz, J. A. C. Bland, L. J. Heyderman, F. Nolting, A. Pavlovska, E. Bauer, S. Cherifi, S. Heun, and A. Locatelli, Appl. Phys. Lett. **85**, 5637 (2004).
[11] R. D. McMichael and M. J. Donahue, IEEE Trans. Magn. **33**, 4167 (1997).
[12] M. F. Lai, Z. H. Wei, C. R. Chang, J. C. Wu, J. H. Kuo, and J. Y. Lai, Phys. Rev. B **67**, 104419 (2003).
[13] R. Wieser, U. Nowak, and K. D. Usadel, Phys. Rev. B **69**, 64401 (2004).
[14] D. Buntinx, A. Volodin, and C. Van Haesendonck, J. Magn. Magn. Mater. **272-276**, e1269 (2004).
[15] Micromagnetic simulation was done with the OOMMF code, which is available at http://math.nist.gov/oommf